


Polarimetry of M-type asteroids in the context of their surface composition

I. Belskaya¹ , A. Berdyugin², Yu. Krugly¹, Z. Donchev³, A. Sergeev¹, R. Gil-Hutton⁴, S. Mykhailova¹, T. Bonev³, V. Piirola², S. Berdyugina⁵, M. Kagitani⁶, and T. Sakanoi⁶

¹ V. N. Karazin Kharkiv National University, 4 Svobody Sq., Kharkiv 61022, Ukraine
e-mail: irina@astron.kharkov.ua

² Department of Physics and Astronomy, University of Turku, 20014 Turku, Finland

³ Institute of Astronomy and NAO, Bulgarian Academy of Sciences, Sofia, Bulgaria

⁴ Planetary Science Group, Universidad Nacional de San Juan and CONICET, Av. José I. de la Roza 590 (O), J5402DCS Rivadavia, San Juan, Argentina

⁵ Leibniz-Institut für Sonnenphysik, 79104 Freiburg, Germany

⁶ Graduate School of Science, Tohoku University, Aoba-ku, Sendai 980-8578, Japan

Received 30 November 2021 / Accepted 15 March 2022

ABSTRACT

Aims. We aim to investigate how polarimetric observations can improve our understanding of the nature and diversity of M/X-type asteroids.

Methods. Polarimetric observations of the selected M/X-type asteroids were carried out at the Tohoku 0.6-m telescope at Haleakala Observatory, Hawaii (simultaneously in *BVR* filters), the 2-m telescope of the Bulgarian National Astronomical Observatory in Rozhen (in *R* filter), and the 2.15-m telescope of the Complejo Astronómico El Leoncito (CASLEO), Argentina (in *V* filter). We analysed the polarimetric characteristics of M/X-type asteroids along with the available data obtained by other techniques.

Results. New polarimetric observations of 22 M/X-type asteroids combined with published observations provide a data set of 41 asteroids for which the depth of a negative polarisation branch and/or inversion angle were determined. We found that the depth of the negative polarisation branch tends to increase with decreasing steepness of the near-infrared spectra. Asteroids with a deeper negative polarisation branch tend to have a higher radar circular polarisation ratio. We show that, based on the relationship of the depth of the negative polarisation branch and inversion angle, two main sub-types can be distinguished among M-type asteroids. We suggest that these groups may be related to different surface compositions similar to (1) irons and stony-irons and (2) enstatite and iron-rich carbonaceous chondrites.

Key words. minor planets, asteroids: general – techniques: polarimetric

1. Introduction

Using the letter M (metal) to classify several asteroids was proposed by Zellner & Gradie (1976) due to the similarity of their polarimetric and spectral properties to iron meteorites. However, possible spectral meteorite analogues of these asteroids included not only iron meteorites but also some types of enstatite chondrites (Chapman et al. 1975). “M type” was one of seven major types in Tholen’s taxonomy that was well separated from other types by featureless spectra and moderate surface albedo (Tholen 1989). In recent classifications, M type is a part of the X complex, which includes all asteroids with featureless spectra regardless of their albedo (Bus & Binzel 2002; Lazzaro et al. 2004; DeMeo et al. 2009).

Initially, it was believed that M-type asteroids could be the remnants of the metal cores of differentiated planetesimals, and this caused a great interest in their study. Numerous observations of M-type asteroids by various techniques revealed that M-type includes asteroids of diverse composition. Rivkin et al. (1995, 2000) found absorption features at 3 μm that were inconsistent with a metal-dominated composition for 10 out of 27 M-type asteroids. Spectroscopic surveys of M/X-type

asteroids revealed a variety of spectral behaviours, as well as weak absorption features in the near-infrared wavelength range (Clark et al. 2004; Fornasier et al. 2010, 2011; Ockert-Bell et al. 2008; 2010; Hardersen et al. 2011; Neeley et al. 2014). In total, the near-infrared spectra were measured for about 45 M-type asteroids. Spectral data obtained for the same asteroid by different authors often showed inconsistencies in the identification of weak absorption bands (Fornasier et al. 2010; Hardersen et al. 2011). Radar studies of M/X-type asteroids were summarised by Shepard et al. (2010, 2015). They found that the radar albedos for 11 of 29 measured M-type asteroids matched a metal-dominated composition. A joint analysis of spectroscopic and radar observations of M-type asteroids revealed some inconsistency in their compositional interpretations (Neeley et al. 2014; Shepard et al. 2015).

One more remote sensing technique which efficiently constrains physical properties of atmosphereless bodies surfaces is polarimetry. The degree of linear polarisation P_r of sunlight scattered by an asteroid’s surface is usually defined in terms of the differences between the intensities of the components of the light beam polarised along the planes perpendicular and parallel to the scattering plane. At small phase angles, the latter component

dominates, which leads to the so-called negative polarisation branch in the phase-angle dependence of linear polarisation P_r (α). The parameter P_{\min} characterises the depth of the negative polarisation branch, and the inversion angle α_{inv} , at which the sign of P_r changes, characterises its width. The relationship between P_{\min} and α_{inv} is considered as indicative of an asteroid's surface texture and composition (Dollfus et al. 1989; Belskaya et al. 2017). Dollfus et al. (1979) concluded that the polarimetric parameters of M-type asteroids are compatible with metallic bodies. This conclusion was made by comparing the polarimetric parameters of four M-type asteroids with laboratory data for iron meteorites and various metallic samples. Lupishko & Belskaya (1989) showed that such an interpretation was not unique since some types of ordinary chondrites exhibited polarimetric properties similar to M-type asteroids. Gil-Hutton (2007) carried out the polarimetric survey of M-type asteroids and obtained data on 26 asteroids. Combining obtained and previously published data, the polarimetric parameters P_{\min} and/or α_{inv} were estimated for only 12 asteroids. Gil-Hutton (2007) found that several of them have an M-type controversial taxonomic classification, and the group of asteroids showing in their spectra's 3 μm hydration band (Rivkin et al. 1995; 2000) has polarimetric parameters that are different from those without that feature.

Recent interest in studying metal-rich asteroids increased after the largest M-type asteroid, (16) Psyche, was selected as a target of the forthcoming NASA space mission, which is expected to launch in 2022. Intense pre-flight observations of (16) Psyche have not resolved contradictions in understanding Psyche's composition (e.g. Elkins-Tanton et al. 2020).

The present work aims to explore how polarimetry can complement previous analysis of M/X-type asteroids based on spectral and radar data. The results of new polarimetric observations are presented in Sect. 2. Section 3 describes the determination of polarimetric parameters combining new and published data on M-type asteroids. Section 4 is devoted to the results of searching for correlations between polarimetric parameters and other characteristics. Finally, in Sect. 5 we try to answer the following question: what can polarimetry tell us about the nature of M-type asteroids?

2. Observations

For our observations, we selected targets from the list of asteroids classified as M types by Tholen (1989) or as X complexes in other available classifications (Bus & Binzel 2002; Lazzaro et al. 2004, DeMeo et al. 2009), which have moderate surface albedo from 0.1 to 0.35 according to Akari data (Usui et al. 2011; Alí-Lagoa et al. 2018) and/or WISE data (Masiero et al. 2011; Mainzer et al. 2016). The main purpose of our observations was to determine the values of polarimetric parameters P_{\min} and the inversion angle α_{inv} . Observations were carried out using telescopes at three different observational sites: the remotely controlled Tohoku 0.6-m telescope at the Haleakala Observatory, Hawaii, the 2-m telescope of the Bulgarian National Astronomical Observatory in Rozhen, and the 2.15-m telescope of the CASLEO, Argentina. We obtained polarimetric measurements of 22 asteroids from May 2018 to November 2021. Observations of 11 asteroids were carried out simultaneously in *BVR* filters, while 11 other asteroids were observed either in the *V* or *R* filter. Below, we briefly characterise the specificities of the observations carried out with each instrument.

Observations at the Haleakala Observatory were carried out at the Tohoku 0.6-m telescope equipped with high-precision Dipol-2 polarimeter. This instrument has three CCD cameras

and is capable of simultaneously measuring linear polarisation in the *BVR* pass bands. To control instrumental polarisation, observations of non-polarised (more than 20 stars per typical observing run) and strongly polarised standard stars have been carried out. The magnitude of instrumental polarisation in all pass-bands is $\leq 10^{-4}$. The description of the polarimeter, data acquisition, and data reduction can be found in Pirola et al. (2014, 2020).

Observations at the Bulgarian National Astronomical Observatory in Rozhen were conducted with the two-channel focal reducer (FoReRo2) (Jockers et al. 2000) installed on the Cassegrain focus of the 2-m telescope at the Rozhen Observatory. In polarimetric mode, FoReRo2 is equipped with a $\lambda/2$ retarder wave plate. A Wollaston prism is placed in the parallel beam before the color divider, and thus it feeds both channels, the red and the blue, simultaneously. To measure the linear polarisation of asteroids, we followed the technique described by Bagnulo et al. (2006). Observations were carried out in the *R* band of the Johnson-Cousins system (*R*-channel) with an Andor's iKon-L 936 CCD camera. We obtained a series of CCD frames at different half-wave plate positions rotated with 22.5° steps. The telescope tracking was used to keep a moving asteroid in the centre of the apertures. Each night, we measured two or more polarimetric standard stars with high and low polarisation to control the instrumental polarisation. The instrumental polarisation was less than 0.02%, and the position angle deviation was about 0.5°. The observational data were processed using the standard procedure (Bagnulo et al. 2006).

Observations at CASLEO were carried out with the 2.15 m telescope and using the CASPOL polarimeter. The CASPOL instrument is a polarisation unit inserted in front of a CCD camera that allows high-precision imaging polarimetry. This polarimeter was built following the design of Magalhaes et al. (1996) and uses an achromatic half-wave retarder and a Savart plate as an analyser. The polarimetric measurements and their errors are obtained from a least-squares solution applied to the measurements at different half-wave plate positions. The overall acquisition process and the data reduction pipeline is essentially identical to that previously used in Gil-Hutton et al. (2017).

The observational circumstances and results of our polarimetric observations are presented in Table 1. For each asteroid, we list the mean time of observations in UT, the adopted filter, the phase angle α , the measured polarisation degree P and the position angle θ in the equatorial system, their root-mean-square errors σ_P and σ_θ , the polarisation degree P_r , and the position angle θ_r in the coordinate system referring to the scattering plane, as defined by Zellner & Gradie (1976).

Wavelength dependence. Simultaneous *BVR* measurements obtained for 11 asteroids provide an opportunity to estimate the wavelength dependence of the polarisation degree. The measured polarisation degrees versus phase angle in *BVR* filters for all observed asteroids are shown in Fig. 1a. We found that the differences between measurements in different filters are small and typically fall within the errors of the measurements. To evaluate wavelength dependence we calculated the linear slope of the polarisation degree in the wavelength range of 0.44–0.64 μm for each observed asteroid. These slopes are plotted in Fig. 1b as a function of the phase angle at which they were measured. Observed asteroids typically show a small negative slope, which means that the negative polarisation branch is deeper with increasing wavelength. This trend is consistent with previous findings for M-type asteroids in the wider wavelength range (Belskaya et al. 2009). For two asteroids, (755) Quintilla

Table 1. Observational circumstances and results of our polarimetric observations.

Asteroid	Date, UT	Filter	α , deg	P , %	σ_P , %	θ , deg	σ_θ , deg	P_r , %	θ_r , deg
(22) Kalliope ⁽¹⁾	2021 11 08.90	R	18.7	0.315	0.049	92.8	4.5	-0.315	90.0
(69) Hesperia ⁽²⁾	2018 08 07.34	V	17.3	0.46	0.08	59.4	2.2	-0.45	84.1
(77) Frigga ⁽¹⁾	2020 11 17.13	R	23.3	0.179	0.045	19.2	7.2	0.179	177.9
(129) Antigone ⁽¹⁾	2021 11 08.99	R	7.97	0.970	0.035	36.3	1.0	-0.967	92.2
(135) Hertha	2021 03 04.35	B	15.9	0.603	0.037	97.4	1.7	-0.600	87.1
(135) Hertha	2021 03 04.35	V	15.9	0.734	0.052	98.7	2.0	-0.733	88.4
(135) Hertha	2021 03 04.35	R	15.9	0.641	0.031	96.5	1.4	-0.635	86.2
(135) Hertha	2021 03 18.39	B	18.4	0.305	0.085	94.6	7.8	-0.300	85
(135) Hertha	2021 03 18.39	V	18.4	0.638	0.071	92.3	3.2	-0.617	82.7
(135) Hertha	2021 03 18.39	R	18.4	0.488	0.053	96.5	3.1	-0.485	86.9
(184) Dejepeja	2021 03 15.61	B	18.8	0.268	0.080	63.5	8.4	-0.119	58.2
(184) Dejepeja	2021 03 15.61	V	18.8	0.507	0.113	73.2	6.3	-0.363	67.9
(184) Dejepeja	2021 03 15.61	R	18.8	0.552	0.043	60.8	2.2	-0.198	55.5
(184) Dejepeja	2021 03 20.61	B	18.6	0.240	0.078	96.1	8.4	-0.108	58.4
(184) Dejepeja	2021 03 20.61	V	18.6	0.548	0.117	84.4	6.0	-0.510	79.3
(184) Dejepeja	2021 03 20.61	R	18.6	0.324	0.084	99.6	7.3	-0.320	94.5
(201) Penelope ⁽²⁾	2018 05 18.05	V	17.1	0.32	0.06	108.6	3.0	-0.31	83.0
(224) Oceana ⁽²⁾	2021 08 07.28	V	15.8	0.58	0.19	59.0	9.2	-0.55	81.0
(250) Bettina	2021 03 19.26	B	20.8	0.080	0.042	39.0	13.9	-0.013	49.7
(250) Bettina	2021 03 19.26	V	20.8	0.171	0.051	62.1	8.2	-0.141	72.8
(250) Bettina	2021 03 19.26	R	20.8	0.146	0.032	75.0	6.2	-0.144	85.7
(337) Devosa ⁽¹⁾	2021 11 08.94	R	5.9	1.079	0.031	8.0	1.0	-1.079	90.8
(347) Pariana	2021 03 15.58	B	24.8	0.354	0.049	175.5	4.0	0.336	170.9
(347) Pariana	2021 03 15.58	V	24.8	0.487	0.098	7.8	5.7	0.484	3.2
(347) Pariana	2021 03 15.58	R	24.8	0.416	0.057	0.7	3.9	0.412	176.1
(347) Pariana	2021 03 19.59	R	24.5	0.437	0.070	1.6	4.6	0.436	177.8
(347) Pariana	2021 03 19.59	V	24.5	0.336	0.074	165.9	6.2	0.273	162.1
(347) Pariana	2021 03 19.59	R	24.5	0.379	0.045	176.9	3.4	0.368	173.1
(369) Aeria ⁽²⁾	2018 05 18.26	V	11.2	0.85	0.07	73.6	1.9	-0.82	82.4
(369) Aeria ⁽¹⁾	2020 11 17.15	R	20.9	0.052	0.055	121.1	30.3	-0.049	100.4
(382) Dodona	2021 03 18.45	R	11.5	0.738	0.082	98.0	3.2	-0.725	84.6
(382) Dodona	2021 03 18.45	V	11.5	0.979	0.105	102.2	3.2	-0.978	88.8
(382) Dodona	2021 03 18.45	R	11.5	1.017	0.075	102.3	2.1	-1.016	88.9
(441) Bathilde ⁽¹⁾	2021 11 05.09	R	20.9	0.137	0.323	81.3	67.5	-0.080	62.9
(441) Bathilde ⁽¹⁾	2021 11 09.15	R	21.2	0.248	0.093	115.9	10.7	-0.241	97.0
(678) Fredegundis	2021 03 04.52	R	6.8	0.810	0.050	136.9	1.8	-0.809	88.5
(678) Fredegundis	2021 03 04.52	V	6.8	0.968	0.067	137.7	2.0	-0.968	89.3
(678) Fredegundis	2021 03 04.52	R	6.8	0.881	0.042	135.3	1.4	-0.876	86.9
(741) Botolphia	2021 03 15.50	R	8.7	0.907	0.099	77.1	3.1	-0.907	89.1
(741) Botolphia	2021 03 15.50	V	8.7	1.259	0.166	76.6	3.8	-1.257	88.6
(741) Botolphia	2021 03 15.50	R	8.7	1.129	0.101	73.5	2.6	-1.115	85.5
(741) Botolphia	2021 03 22.44	R	6.5	0.962	0.055	60.1	1.6	-0.962	90.1
(741) Botolphia	2021 03 22.44	V	6.5	1.003	0.058	57.1	1.7	-0.998	87.1
(741) Botolphia	2021 03 22.44	R	6.5	0.967	0.041	59.7	1.2	-0.967	89.7
(755) Quintilla	2021 05 08.34	R	8.7	0.997	0.048	113.8	1.4	-0.987	86.0
(755) Quintilla	2021 05 08.34	V	8.7	1.043	0.069	114.8	1.9	-1.037	87.0
(755) Quintilla	2021 05 08.34	R	8.7	1.155	0.034	115.0	0.8	-1.149	87.2
(755) Quintilla	2021 05 13.34	R	10.6	1.070	0.061	114.1	1.6	-1.066	87.4
(755) Quintilla	2021 05 13.34	V	10.6	1.186	0.080	116.5	1.9	-1.186	89.8
(755) Quintilla	2021 05 13.34	R	10.6	1.141	0.053	115.2	1.3	-1.139	88.5
(755) Quintilla	2021 06 01.37	R	16.3	0.869	0.072	112.7	2.4	-0.868	88.4
(755) Quintilla	2021 06 01.37	V	16.3	0.676	0.108	109.1	4.5	-0.665	84.8
(755) Quintilla	2021 06 01.37	R	16.3	0.588	0.056	110.1	2.7	-0.582	85.8
(758) Mancunia	2021 05 17.40	R	8.3	0.905	0.070	81.5	2.2	-0.897	86.2
(758) Mancunia	2021 05 17.40	V	8.3	1.307	0.130	85.9	2.8	-1.307	90.6
(758) Mancunia	2021 05 17.40	R	8.3	1.183	0.061	82.1	1.5	-1.176	86.8
(758) Mancunia	2021 05 18.42	R	8.1	1.203	0.064	83.7	1.5	-1.201	88.5
(758) Mancunia	2021 05 18.42	V	8.1	1.039	0.097	82.6	2.7	-1.035	87.4

Table 1. continued.

Asteroid	Date, UT	Filter	α , deg	P , %	σ_P , %	θ	σ_θ , deg	P_r , %	θ_r , deg
(758) Mancunia	2021 05 18.42	R	8.1	1.195	0.067	81.6	1.6	-1.186	86.4
(779) Nina ⁽¹⁾	2021 11 08.78	R	10.7	1.026	0.043	49.2	1.2	-1.021	92.8
(785) Zwetana	2021 03 19.31	R	24.0	0.256	0.077	114.3	8.3	-0.247	97.8
(785) Zwetana	2021 03 19.31	V	24.0	0.054	0.084	1.0	28.8	0.046	164.5
(785) Zwetana	2021 03 19.31	R	24.0	0.182	0.058	15.4	8.9	0.182	178.9
(872) Holda	2021 05 08.45	R	11.3	0.991	0.050	74.9	1.5	-0.979	85.5
(872) Holda	2021 05 08.45	V	11.3	0.995	0.059	76.2	1.7	-0.989	86.8
(872) Holda	2021 05 08.45	R	11.3	1.033	0.041	77.0	1.2	-1.029	87.6
(872) Holda	2021 05 13.44	R	9.4	1.053	0.052	68.7	1.4	-1.030	84.0
(872) Holda	2021 05 13.44	V	9.4	0.970	0.058	73.6	1.7	-0.969	88.9
(872) Holda	2021 05 13.44	R	9.4	1.238	0.040	70.7	0.9	-1.226	86.0
(872) Holda	2021 05 15.42	R	8.7	1.132	0.054	71.1	1.4	-1.131	88.8
(872) Holda	2021 05 15.42	V	8.7	1.110	0.100	71.5	2.6	-1.110	89.2
(872) Holda	2021 05 15.42	R	8.7	1.081	0.049	72.6	1.3	-1.081	90.3
(1222) Tina ⁽¹⁾	2021 11 04.75	R	23.12	0.875	0.158	171.2	5.2	0.873	2.1
(1222) Tina ⁽¹⁾	2021 11 08.70	R	23.52	0.810	0.053	174.2	1.9	0.786	6.9

Notes. ⁽¹⁾Observations at Rozhen. ⁽²⁾Observations at CASLEO.

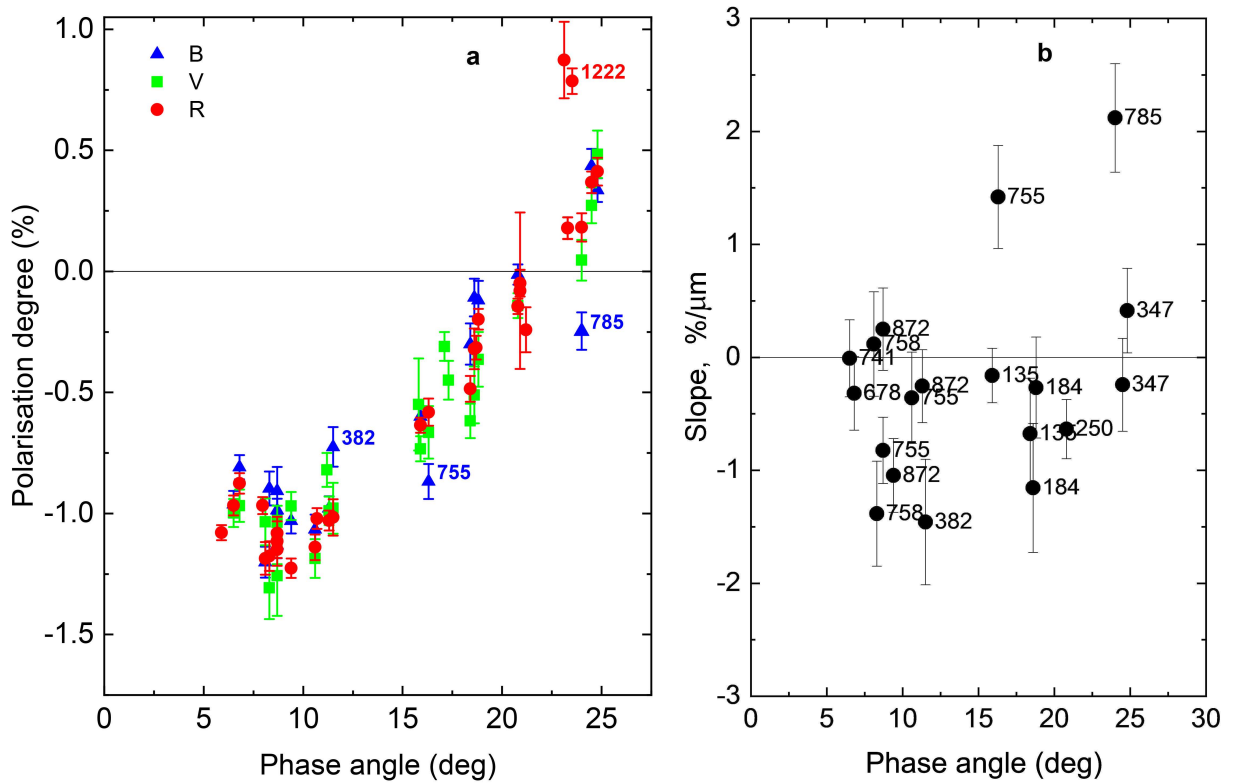


Fig. 1. Polarisation degree in the B , V , R filters (a) and polarisation spectral slope (b) as a function of phase angle for the observed asteroids. Asteroids with large deviations of the measured polarisation degree from typical values are marked with their numbers in Fig. 1a.

and (785) Zwetana, measurements at the phase angle $\alpha > 15^\circ$ revealed an opposite trend, and whether this trend is real or not will require further verification.

3. Determination of polarimetric parameters

We analysed the new observational data together with the available literature data on M/X-type asteroids. The published data

and all relevant references are given in the catalogues of asteroid polarimetry (Lupishko 2019, Gil-Hutton 2017). In case of a discrepancy between the data obtained by different authors, we carefully examined original publications. Individual polarimetric phase curves of the observed asteroids including both new and already published data are shown in Fig. 2. For some asteroids, we combined observations in V and R filters, since the expected differences of the polarisation degree measured in these filters are within the accuracy of observational data. The

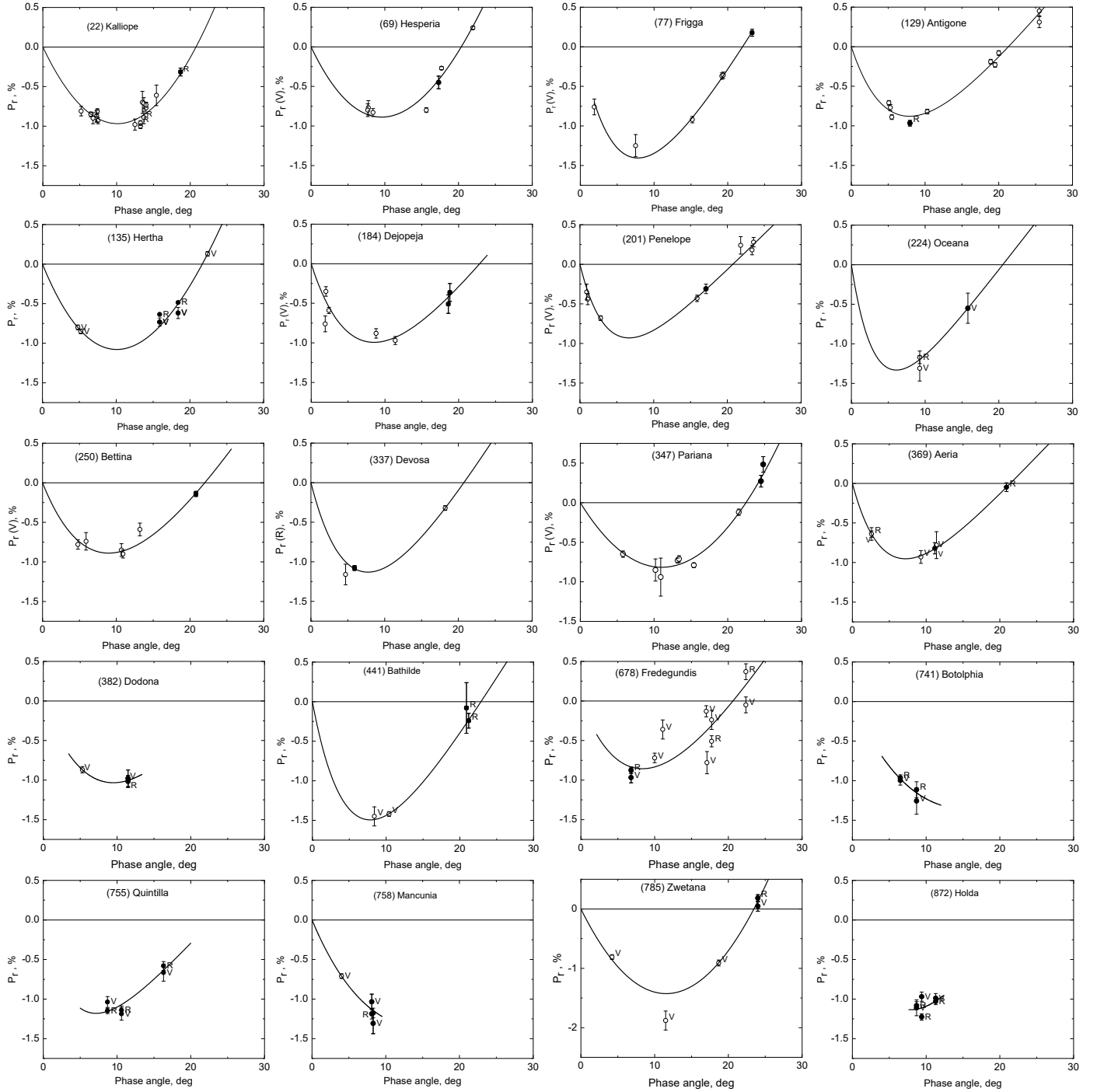


Fig. 2. Polarisation-phase curves of the measured asteroids. New observations are shown by filled symbols and previously published data are shown by open symbols. The line shows the best fit of the exponential-linear function (Kaasalainen et al. 2003; Muinonen et al. 2009).

filter in which observations were obtained is indicated in each figure.

For fitting the data, we used the exponential-linear function (Kaasalainen et al. 2003; Muinonen et al. 2009) in the following form:

$$P_r = A(e^{-\alpha/B} - 1) + C \cdot \alpha,$$

where α is the phase angle expressed in degrees, and A , B , and C are free parameters. The function is known to work well up to $\alpha \leq 30^\circ$ (Muinonen et al. 2009). We used the Levenberg-Marquardt algorithm to calculate the best-fitting parameters A ,

B , and C , and their errors were obtained using a Monte Carlo simulation. With these parameters, it is possible to calculate the usual polarimetric parameters and estimate their uncertainties by a propagation of errors. The parameters P_{\min} and inversion angle α_{inv} were found using the procedure described in the paper by Muinonen et al. (2009). For objects with few measurements, we fixed the parameter C within the range of 0.1–0.15. These values of polarimetric slope parameter are inherent for moderate albedo asteroids with geometric albedos $p_V \sim 0.1$ –0.2 according to empirical polarimetric slope-albedo relationships (Cellino et al. 2015; Lupishko 2018). In the case of a single available

Table 2. Polarimetric parameters and other characteristics of M/X-type asteroids.

Asteroid ⁽¹⁾	Type (Tholen/Bus-DeMeo)	p_V (Akari)	p_V (WISE)	$ P_{\min} $	α_{inv}	NIR slope ⁽²⁾
(16) Psyche	M/Xk	0.19 ± 0.08	–	1.06 ± 0.05	22.3 ± 0.6	0.17 ± 0.07
(21) Lutetia	M/Xc	0.15 ± 0.03	–	1.32 ± 0.07	25.0 ± 0.4	−0.03 ± 0.02
(22) Kalliope	M/X	0.22 ± 0.04	0.17 ± 0.01	0.97 ± 0.07	21.0 ± 1.0	0.16 ± 0.02
(55) Pandora	M/Xk	0.33 ± 0.07	–	0.97 ± 0.06	20.6 ± 0.8	0.15 ± 0.05
(69) Hesperia	M/Xk	0.12 ± 0.03	–	0.85 ± 0.10	20.5 ± 0.8	0.12 ± 0.04
(75) Eurydike	M/Xk	0.11 ± 0.02	0.12 ± 0.03	–	20.1 ± 0.8	–
(77) Frigga	MU/Xe	0.13 ± 0.03	0.23 ± 0.03	1.30 ± 0.15	22.0 ± 0.5	0.07 ± 0.03
(92) Undina	X/Xk	0.25 ± 0.05	–	0.80 ± 0.15	–	–
(97) Klotho	M/Xc	0.18 ± 0.04	0.25 ± 0.04	1.35 ± 0.15	22.6 ± 0.9	−0.03 ± 0.03
(110) Lydia	M/Xk	0.18 ± 0.04	0.17 ± 0.02	0.90 ± 0.10	–	0.13 ± 0.03
(125) Liberatrix	M/X	0.29 ± 0.06	0.18 ± 0.04	0.85 ± 0.15	20.4 ± 0.9	0.20 ± 0.06
(129) Antigone	M/X	0.17 ± 0.03	0.15 ± 0.06	0.90 ± 0.10	21.4 ± 0.6	0.18 ± 0.05
(132) Aethra	M/Xe	0.17 ± 0.03	–	1.10 ± 0.15	19.5 ± 0.5	–
(135) Hertha	M/Xk	0.17 ± 0.03	0.18 ± 0.03	0.95 ± 0.10	21.6 ± 0.8	0.13 ± 0.03
(161) Athor	M/Xc	0.23 ± 0.05	–	–	18.9 ± 1.0	–
(184) Dejopeja	X/X	0.17 ± 0.03	0.22 ± 0.02	1.00 ± 0.10	–	0.17 ± 0.05
(201) Penelope	M/Xk	0.19 ± 0.04	0.10 ± 0.03	–	20.9 ± 0.8	–
(216) Kleopatra	M/Xe	0.17 ± 0.03	0.15 ± 0.03	1.00 ± 0.10	21.2 ± 1.0	0.16 ± 0.02
(224) Oceana	M/X,T ⁽³⁾	0.19 ± 0.04	0.24 ± 0.05	1.20 ± 0.15	–	0.05 ± 0.01
(250) Bettina	M/Xk	0.14 ± 0.03	0.11 ± 0.02	0.90 ± 0.12	22.0 ± 0.9	0.21 ± 0.02
(325) Heidelberga	M/–	0.10 ± 0.02	–	0.95 ± 0.15	–	0.17 ± 0.05
(337) Devosa	X/Xk	0.12 ± 0.02	–	1.15 ± 0.12	–	0.12 ± 0.03
(338) Budrosa	M/Xk	0.14 ± 0.03	0.28 ± 0.05	0.98 ± 0.10	–	0.12 ± 0.01
(347) Pariana	M/–	0.17 ± 0.03	0.22 ± 0.05	0.95 ± 0.15	22.2 ± 0.8	0.18 ± 0.03
(359) Georgia	CXM/Xk	0.13 ± 0.03	–	–	20.8 ± 0.6	–
(369) Aeria	M/–	0.15 ± 0.03	0.17 ± 0.04	0.95 ± 0.10	21.1 ± 0.9	0.19 ± 0.08
(382) Dodona	M/–	0.19 ± 0.04	0.13 ± 0.02	1.03 ± 0.10	–	0.14 ± 0.03
(441) Bathilde	M/Xk	0.16 ± 0.03	0.20 ± 0.01	1.40 ± 0.10	22.8 ± 1.0	0.04 ± 0.03
(504) Cora	–/X	0.21 ± 0.04	0.34 ± 0.05	1.00 ± 0.10	–	–
(558) Carmen	M/Xk ⁽³⁾	0.14 ± 0.03	0.13 ± 0.04	0.80 ± 0.06	–	0.20 ± 0.09
(678) Fredegundis	–/X	0.19 ± 0.04	0.34 ± 0.06	0.90 ± 0.08	20.6 ± 1.0	0.12 ± 0.02
(741) Botolphia	X/X	0.20 ± 0.04	–	1.15 ± 0.10	–	–
(755) Quintilla	M/–	0.22 ± 0.09	0.12 ± 0.01	1.15 ± 0.10	–	0.04 ± 0.08
(757) Portlandia	XF/Xk	0.13 ± 0.03	0.22 ± 0.03	1.00 ± 0.20	16.6 ± 0.7	0.05 ± 0.03
(758) Mancunia	X/–	0.11 ± 0.02	0.12 ± 0.02	1.25 ± 0.10	–	0.08 ± 0.03
(779) Nina	–/X	0.14 ± 0.03	0.16 ± 0.02	1.00 ± 0.10	–	–
(785) Zwetana	M/Cb	0.13 ± 0.03	–	1.88 ± 0.20	24.0 ± 0.6	0.21 ± 0.02
(796) Sarita	XD/X	0.23 ± 0.05	0.21 ± 0.03	1.00 ± 0.10	21.0 ± 1.0	0.20 ± 0.08
(849) Ara	M/–	0.30 ± 0.06	0.13 ± 0.04	0.95 ± 0.10	–	0.21 ± 0.08
(872) Holda	M/X	0.17 ± 0.03	0.24 ± 0.03	1.13 ± 0.10	–	0.13 ± 0.02
(1222) Tina	–/X	0.09 ± 0.02	0.20 ± 0.05	–	~20	–

Notes. ⁽¹⁾Asteroids observed in the present work are marked in bold. ⁽²⁾The spectral slope in the 1.7–2.4 μm wavelength range calculated using the published data by Clark et al. (2004); Fornasier et al. (2010), Ockert-Bell et al. (2008; 2010); Hardersen et al. (2011); and Neeley et al. (2014). ⁽³⁾Type from Lazzaro et al. (2004).

measurement in the vicinity of P_{\min} (at phase angles of 7–11°), we preferred to use the measured value as P_{\min} rather than the value derived from the fitting curve. The inversion angle was determined only when the measurements were available at phase angles close to the inversion angle ($\alpha \geq 19^\circ$). We would like to mention that different ways of determining the polarimetric parameters give consistent results within the assigned uncertainties and do not affect our further conclusions.

The best-fitted curves are plotted in Fig. 2. Data for the asteroids (779) Nina and (1222) Tina are not presented in Fig. 2 since they have only two points each. Typically, the deviation of observational data from the fitting function is within the errors

of measurements. Only two asteroids from our sample, (678) Fredegundis and (785) Zwetana, show a large scatter of data points (see Fig. 2). Such a scatter is difficult to explain by possible variations of polarisation degree over the surface, since the expected variations for main belt asteroids are small (e.g. Cellino et al. 2016). There are most likely technical problems with some measurements.

With our new observations, at least one of two polarimetric parameters P_{\min} or α_{inv} was estimated for the first time or revised for all considered asteroids. The determined polarimetric parameters of these asteroids (marked in bold) are given in Table 2. We also included 19 asteroids of M/X-type for which

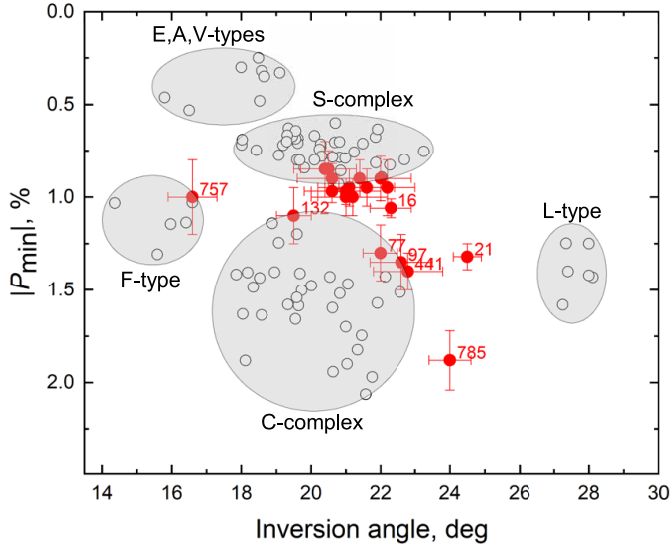


Fig. 3. Relationship of P_{\min} and α_{inv} for asteroids of different composition types. M-type asteroids are shown as filled circles.

polarimetric parameters can be determined based on previously published data available in catalogues of asteroid polarimetry (Lupishko 2019, Gil-Hutton 2017). The observations in V or R filters of each asteroid were fitted by the described above fitting procedure to determine P_{\min} and α_{inv} . Thus, we obtained a homogeneous data set of polarimetric parameters for 41 M/X-type asteroids presented in Table 2. Table 2 also contains their types according to the Tholen (1989) and Bus-DeMeo classification schemes (Bus & Binzel 2002; DeMeo et al. 2009), albedos from Akari data (Alí-Lagoa et al. 2018) and WISE data (Mainzer et al. 2016), and the spectral slopes in the 1.7–2.4 μm wavelength range. The spectral slopes were calculated from the available near-infrared spectra of these asteroids obtained by Clark et al. (2004); Fornasier et al. (2010), Ockert-Bell et al. (2008, 2010); Hardersen et al. (2011); and Neeley et al. (2014) (see Sect. 4.4 for details).

In total, 41 asteroids are listed in Table 2. The data set includes 29 asteroids classified as M types in Tholen’s classification (Tholen 1989), which is about 70% of all asteroids classified as M types, and 12 asteroids classified as X types in the available classifications (Tholen 1989; Bus & Binzel 2002; Lazzaro et al. 2004; DeMeo et al. 2009).

4. Search for relationships

We used the data set of polarimetric parameters of M-type asteroids (Table 2) to search for relationships between the parameters characterising their properties obtained by various techniques.

4.1. P_{\min} versus inversion angle

Table 2 contains 20 asteroids for which both polarimetric parameters P_{\min} and α_{inv} were determined. The relationship between these two parameters characterising the negative polarisation branch is shown in Fig. 3. For comparison, we plotted the data for other composition types based on the catalogue of polarimetric parameters from Gil-Hutton (2017). The polarimetric parameters were calculated in the same way, by fitting the observational data with the exponential-linear function.

We found that asteroids classified as M types (or moderate albedo X types) have a greater scatter of polarimetric parameters

compared to other types (Fig. 3). M-type asteroids can be divided into two main sub-groups. The first sub-group of asteroids with $|P_{\min}| \sim 0.9\text{--}1\%$ and $\alpha_{\text{inv}} \sim 20\text{--}22^\circ$ is located between the S complex and the C complex and looks like a continuation of the S complex. Several M asteroids fall into the S complex. The second sub-group of asteroids with $|P_{\min}| \geq 1.2\%$ and inversion angle $>22^\circ$ fall between C-complex and L-type asteroids.

Two asteroids of our sample, (757) Portlandia and (785) Zwetana, present extreme polarimetric properties. Asteroid (757) Portlandia shows a very small inversion angle typical of low-albedo F-type asteroids (Belskaya et al. 2005). Moreover, this asteroid was initially classified as XF by Tholen (1989), but its geometric albedo of 0.13 (Akari) or 0.22 (WISE) contradicts this classification. Most likely, the albedo is incorrect and (757) Portlandia belongs to a low-albedo F type. Asteroid (785) Zwetana shows a very deep negative polarisation branch incompatible with its moderate albedo (0.13). It was classified as M by Tholen (1989) and Cb by Bus & Binzel (2002) and DeMeo et al. (2009). Further observations of (785) Zwetana are needed to understand the reasons for its particular properties. We do not consider asteroids (757) Portlandia and (785) Zwetana in our search for correlations with radar and spectral data because of their extreme properties, but we include them in our discussion.

4.2. P_{\min} versus geometric albedo

Albedo is the most important characteristic that distinguishes the M type from the X type. Polarimetry can provide independent albedo estimates based on the well-known correlations between polarimetric parameters and albedo (e.g. Zellner et al. 1977). Albedos can be estimated with an uncertainty of about 20% for $|P_{\min}| \leq 1\%$ (Cellino et al. 2015). The deeper negative polarisation branch can occur for asteroids with a wide range of albedos up to 0.2 and cannot be used for reliable albedo estimates of individual asteroids. In our sample, P_{\min} varies from -0.8 to -1.4% , which corresponds to albedos in the range of 0.08–0.2 according to the available ‘ P_{\min} – albedo’ relations (Cellino et al. 2015; Lupishko 2018). The range of radiometric albedos for the same sample is broader and span from 0.1 to 0.34 (see Table 2). In Fig. 4, we plot the dependence of P_{\min} on radiometric albedos separately for Akari data (Alí-Lagoa et al. 2018) and WISE data (Mainzer et al. 2016). Two lines correspond to the ‘ P_{\min} – albedo’ relationship proposed by Lupishko (2018) and Cellino et al. (2015) to calculate polarimetric albedos. As one can see, radiometric albedos are generally higher than polarimetric albedos and do not show a noticeable trend with P_{\min} . A large scatter of ‘ P_{\min} –radiometric albedo’ dependence can be caused both by possible deviations from the relationship and by underestimated errors of radiometric albedos. This comparison shows that albedos of some asteroids can have significant errors and should be used with caution in their spectral modelling.

4.3. Polarimetric parameters and radar data

High radar albedos are considered indicative of a metal-rich surface (Ostro et al. 1985; Shepard et al. 2008, 2015). Polarimetric data are available for 22 of 29 asteroids classified as M/X types for which radar measurements were obtained. Figure 5 shows the relationships of $|P_{\min}|$ and radar data taken from Shepard et al. (2015). The asteroids with lower radar albedos tend to have a deeper negative polarisation branch, with the exception of asteroid (758) Mancunia (Fig. 5a). On the other hand, asteroids with $|P_{\min}| < 1.1\%$ have diverse radar albedos ranging from low to high values. The correlation of P_{\min}

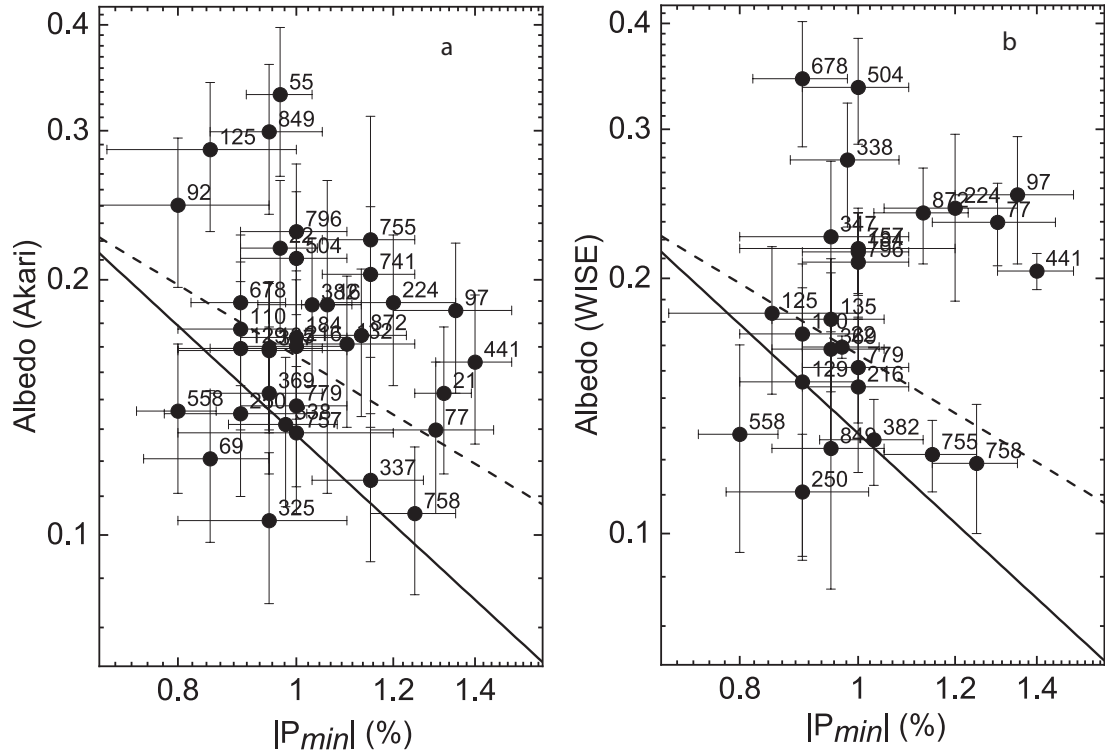


Fig. 4. P_{\min} versus geometric albedos from infrared data (Akari (a) and WISE (b)).

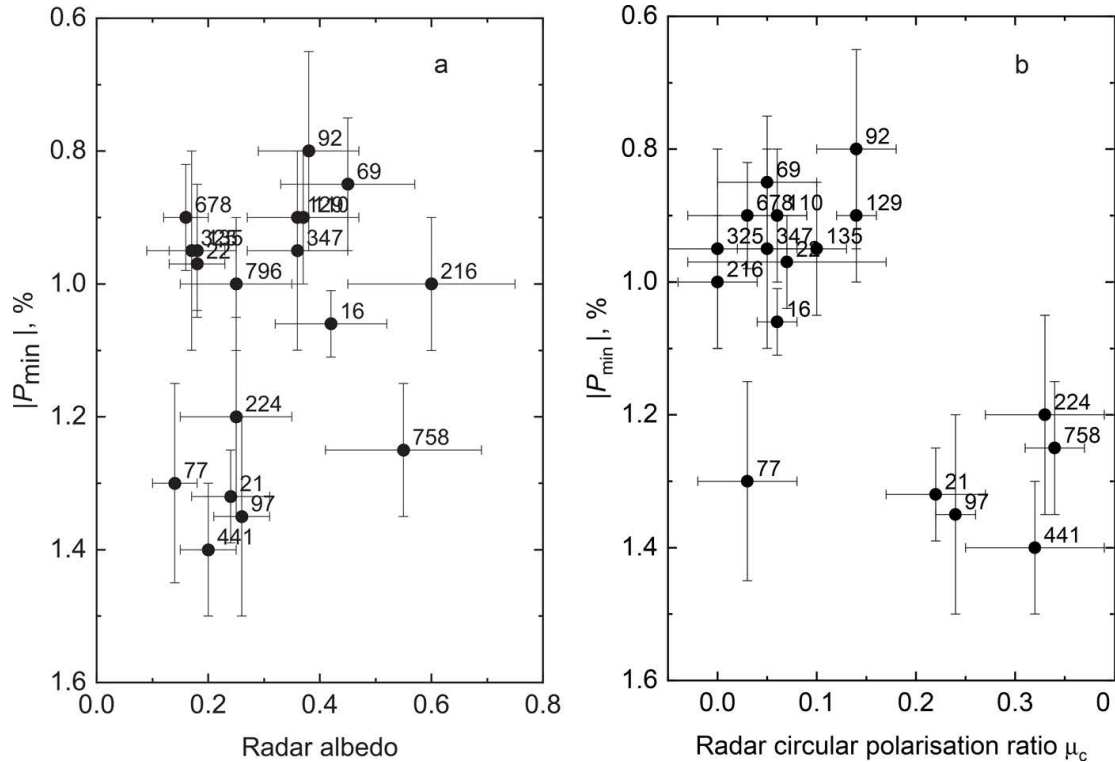


Fig. 5. Relationships of P_{\min} and radar albedos (a) and circular polarisation ratio μ_c (b) for M-type asteroids.

with radar echo's circular polarisation ratio μ_c is more evident (Fig. 5b). Asteroids that have a deeper negative polarisation branch in optical measurements tend to have a higher circular polarisation ratio μ_c . One exception is asteroid (77) Frigga, which is classified as MU in Tholen's taxonomy (Tholen 1989). A strong dependence of circular polarisation ratio on taxonomic

type was found by Benner et al. (2008) for near-Earth asteroids. They assumed that different types of asteroids have distinct differences in their near-surface roughness. Two sub-groups seen in the plot of P_{\min} and radar circular polarisation ratios gave further evidence of diverse taxonomy among M-type asteroids. Both polarimetric parameters P_{\min} and α_{inv} and radar albedos

and μ_c were measured for only 14 asteroids. Although the set is small, two sub-groups seen in the P_{\min} versus α_{inv} plot include asteroids with different radar properties. The asteroids with high radar albedos and small μ_c are located in one sub-group, while the second sub-group contains asteroids with lower radar albedos and higher values of μ_c .

4.4. P_{\min} and spectral slope

Visible spectra of M-type asteroids are characterised by rather similar behaviour. The difference became noticeable at longer wavelengths, which led to the identification several subclasses among X-complex in Bus-DeMeo taxonomy (Bus & Binzel 2002; DeMeo et al. 2009). The near-infrared spectra are available for 31 asteroids from our list of 36 asteroids for which P_{\min} was measured. They were obtained by Clark et al. (2004); Fornasier et al. (2010); Ockert-Bell et al. (2008, 2010); Hardersen et al. (2011), and Neeley et al. (2014). All these spectra are available at the PDS Asteroid Database¹. We used them to calculate spectral slopes in the 1.7–2.4 μm wavelength range. This range was previously used to characterise near-infrared spectra of M/X type asteroids (e.g. Fornasier et al. 2010). We carefully checked each available spectrum for the presence of absorption features. The available spectra are typically featureless in the considered wavelength range. Subtle absorption features reported for several asteroids are present in some spectra but absent from others. We used a simple linear regression to calculate spectral slope and its standard error. In the case of multiple spectra available, we used the most accurate spectra or average value of the slopes. The adopted values of slopes are given in Table 2. They are plotted in Fig. 6 versus $|P_{\min}|$. An inverse correlation is seen between $|P_{\min}|$ and spectral slope in the 1.7–2.4 μm wavelength range. Asteroids with shallower spectral slopes at the near-infrared wavelengths have deeper negative polarisation branches. Such correlation implies that polarimetry is rather sensitive to surface composition of asteroids.

5. Discussion

New polarimetric observations obtained for 22 asteroids of M/X-type combined with available observations provide a data set of 41 asteroids for which at least one of polarimetric parameters P_{\min} or α_{inv} were determined. This data set cover the majority of M/X asteroids that were observed in the previous surveys by spectroscopic and radar techniques (Shepard et al. 2015). So, it becomes possible to add polarimetry as a complimentary technique to previous analysis of M-type asteroids. We did not find noticeable correlation with either the presence or absence of a 3 μm feature or with radar albedos. The most prominent correlation we revealed is the correlation of the depth of negative polarisation and the slope in the near-infrared wavelength range. We also found that asteroids with a deeper negative polarisation branch in optical measurements tend to have higher circular polarisation ratio μ_c . Moreover, the two sub-groups seen in the P_{\min} versus α_{inv} plot are also well distinguished in the plot of P_{\min} and radar circular polarisation ratios. Below we discuss possible interpretation of the diversity of polarimetric parameters among M-type asteroids.

Asteroids with $|P_{\min}| \sim 0.9\text{--}1\%$ and $\alpha_{\text{inv}} \sim 20\text{--}22^\circ$ are (16) Psyche, (22) Kalliope, (55) Pandora, (69) Hesperia, (125) Liberatrix, (129) Antigone, (135) Hertha, (216) Kleopatra, (250) Bettina, (347) Pariana, (369) Aeria, (678) Fredegundis,

¹ <https://sbn.psi.edu/pds/archive/asteroids.html>

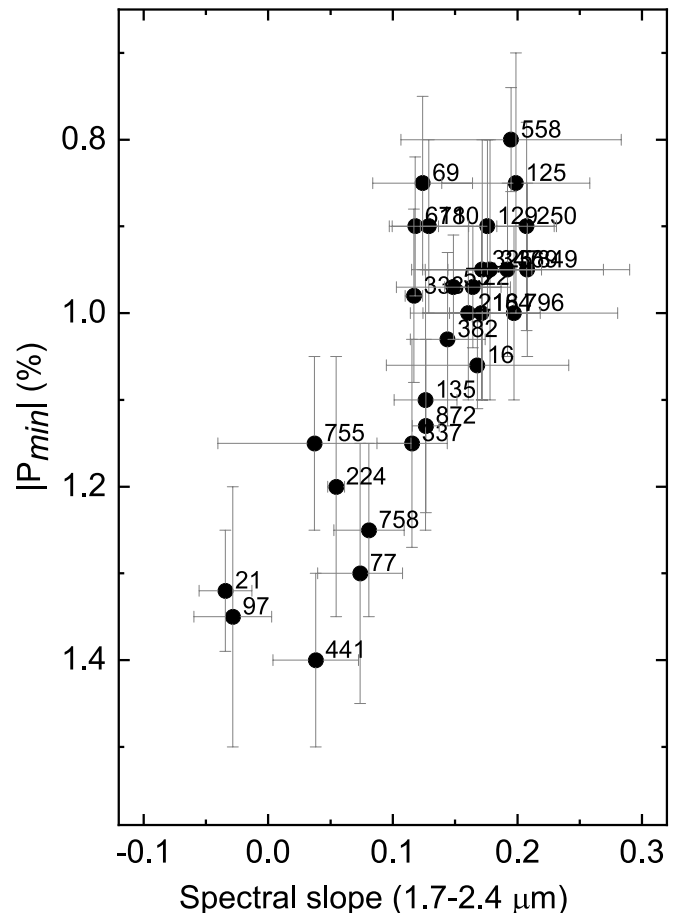


Fig. 6. Relationship of P_{\min} and spectral slope in the 1.7–2.4 μm wavelength range (in reflectance/ μm).

and (796) Sarita. All these asteroids have shown an absorption feature near 0.9 μm , although its centre and depth derived by different authors did not always match (Hardersen et al. 2005; 2011, Fornasier et al. 2010; Ockert-Bell et al. 2008; 2010). For some of these asteroids, the presence of absorption features in the near-infrared wavelength range was reported, but again the data for the same asteroid by different authors were controversial (see Hardersen et al. 2011). Possible meteorite analogues of asteroids with an absorption feature near 0.9 μm include mesosiderites (Vernazza et al. 2009; Hardersen et al. 2011) or silicate-bearing iron meteorites (Hardersen et al. 2011). The bulk density estimations of the largest asteroids from this group are comparable to mesosiderites (Vernazza et al. 2021), but the authors considered stony-iron meteorites as unlikely analogues of these asteroids (Vernazza et al. 2021). All measured main-belt asteroids with high radar albedos (Shepard et al. 2015) also belong to this group.

Asteroids with $|P_{\min}| \geq 1.2\%$ and $\alpha_{\text{inv}} > 22^\circ$ are (21) Lutetia, (77) Frigga, (97) Klotho, (441) Bathilde, and most probably (224) Oceana and (758) Manconia, for which only P_{\min} was measured. These asteroids have flattened spectra in the near-infrared wavelength, have not revealed an absorption band at 0.9 μm , have low or moderate radar albedo (except (758) Manconia) and high circular polarisation ratios (except (77) Frigga). Among these asteroids, (21) Lutetia was well studied during the fly-by of the Rosetta space mission. Some types of carbonaceous chondrites or enstatite chondrites are considered as Lutetia's surface analogues (Barucci et al. 2012). Most probably, all other

asteroids in this group also have a similar analogous among meteorites. This conclusion is also supported by laboratory measurements. The measured samples of carbonaceous chondrites and the enstatite chondrite E4 Abee revealed a deeper negative polarisation branch compared to that for iron meteorites (Zellner et al. 1977; Dollfus et al. 1979; Lupishko & Belskaya 1989). Also, enstatite chondrites tend to have shallower spectral continuum slopes than those of iron meteorites (e.g. Clark et al. 2004).

Asteroids with extreme polarimetric properties include (785) Zwetana and (757) Portlandia. Zwetana is characterised by the deepest negative polarisation branch in our sample. This asteroid revealed several interesting features that placed it outside of typical M types. Available near-infrared spectra demonstrated variable spectral slopes and absorption features detected by some authors (Clark et al. 2004; Ockert-Bell et al. 2010) but not confirmed by others (Fornasier et al. 2010; Hardersen et al. 2011). The considerable variability was also found in radar measurements of (785) Zwetana (Shepard et al. 2008), which was explained by an unusual shape or surface structures of this asteroid (Shepard et al. 2015). The polarimetric observations also revealed an unusually large scatter of data (see Fig. 2). Further observations of (785) Zwetana are needed to explain its unusual surface properties.

Asteroid (757) Portlandia has an extremely small inversion angle previously observed only for low-albedo F-type asteroids (Belskaya et al. 2005). Accurate measurements of its albedo are needed to check whether it belongs to F-type asteroids or if it has unique properties.

Based on a comparison of polarimetric parameters and available information on surface composition of M-type asteroids from other sources, we assume that the sub-groups in the ' $P_{\min} - \alpha_{\text{inv}}$ ' relationship most likely indicate two different surface compositions. Although it is well known that the value of an inversion angle is sensitive to a regolith particle size increasing as the size of particles decreases (e.g. Dollfus et al. 1989), such interpretation is ambiguous. The inversion angle also depends on the surface composition increasing with an increase of the refractive index of the surface material (e.g. see Gil-Hutton & García-Migani 2017). We know an impressive example of the sensitivity of polarimetric parameters to asteroid surface composition. The discovery of anomalous polarimetric properties of asteroid (234) Barbara (Cellino et al. 2006) led to a separate group of 'barbarians' being established. It was later proved that all asteroids of this group belong to the same L-type (Devogèle et al. 2018). Asteroids of other taxonomic types are also grouped in the ' $P_{\min} - \alpha_{\text{inv}}$ ' diagram (Belskaya et al. 2017). Thus, we suggest that two sub-groups of M-type asteroids with different polarimetric characteristics may indicate their different surface compositions, corresponding to two different meteorite analogues, such as (1) irons and stony-irons, and (2) enstatite and high-iron carbonaceous chondrites. Of course, only with additional data it will be possible to confirm or reject this assumption.

6. Conclusions

We obtained new polarimetric observations for 22 M/X-type asteroids and combined them with previously available observations to determine polarimetric parameters characterising the depth and width of a negative polarisation branch. At least one of these polarimetric parameters were determined for 41 asteroids, which cover the majority of M/X-type asteroids observed in the previous surveys by spectroscopic and radar techniques.

The main conclusions from the analysis of polarimetric data and other available data on M-type asteroids can be summarised as follows:

1. M-type asteroids have a wider range of polarimetric parameters as compared to other types, which confirmed a diversity within M-type. Majority of considered asteroids fall into two sub-groups in the plot of polarimetric parameters P_{\min} and α_{inv} . Asteroids (757) Portlandia and (785) Zwetana present extreme cases and most probably do not belong to M-type asteroids;
2. We found a correlation of the depth of negative polarisation and the spectral slope in the near-infrared wavelength range. Asteroids with shallower spectral slopes at the near-infrared wavelengths have deeper negative polarisation branches;
3. Asteroids with deeper negative polarisation branches tend to have higher radar circular polarisation ratios μ_c . Two sub-groups are also well distinguished in the plot of P_{\min} and radar circular polarisation ratios;
4. We suggest that two sub-groups of M-type asteroids with different polarimetric characteristics may have different meteorite analogues, such as (1) irons and stony-irons, and (2) enstatite and high-iron carbonaceous chondrites.

Thus, polarimetry can be an efficient tool in study of X/M-type asteroids. The accuracy of measurements of polarisation degree should be better than 0.1% in order to reveal differences in the polarisation phase curve behaviours of individual asteroids. Further observations are needed to increase the statistics and confirmed our findings.

Acknowledgements. Ukrainian team is supported by the National Research Foundation of Ukraine, grant o. 2020.02/0371 "Metallic asteroids: search for parent bodies of iron meteorites, sources of extraterrestrial resources". Dipol-2 was built in the cooperation between the University of Turku, Finland, and the Leibniz Institute for Solar Physics, Germany, with the support by the Leibniz Association grant SAW-2011-KIS-7. We are grateful to the Institute for Astronomy, University of Hawaii for the observing time allocated for us on the T60 telescope. RGH gratefully acknowledges financial support by CONICET through PIP 112-202001-01227 and San Juan National University by a CICITCA grant for the period 2020–2021. T.B. acknowledges financial support by the National Science Fund in Bulgaria through contract DN 18/13-12.12.2017. We are grateful to all the defenders of Ukraine from the Russian invasion so that we can safely finalize this article.

References

- Alí-Lagoa, V., Müller, T. G., Usui, F., & Hasegawa, S. 2018, *A&A*, **612**, A85
 Bagnulo, S., Boehnhardt, H., Muinonen, K., et al. 2006, *A&A*, **450**, 1239
 Barucci, M. A., Belskaya, I. N., Fornasier, S., et al. 2012, *Planet. Space Sci.*, **66**, 23
 Belskaya, I. N., Shkuratov, Y. G., Efimov, Y. S., et al. 2005, *Icarus*, **178**, 213
 Belskaya, I. N., Lévassieur-Regourd, A.-C., Cellino, A., et al. 2009, *Icarus*, **199**, 97
 Belskaya, I. N., Fornasier, S., Tozzi, G. P., et al. 2017, *Icarus*, **284**, 30
 Benner, L. A. M., Ostro, S. J., Magri, C., et al. 2008, *Icarus*, **198**, 294
 Bus, S. J., & Binzel, R. P. 2002, *Icarus*, **158**, 146
 Cellino, A., Belskaya, I. N., Bendjoya, P., et al. 2006, *Icarus*, **180**, 565
 Cellino, A., Bagnulo, S., Gil-Hutton, R., et al. 2015, *MNRAS*, **451**, 3473
 Cellino, A., Ammannito, E., Magni, G., et al. 2016, *MNRAS*, **456**, 248
 Chapman, C. R., Morrison, D., & Zellner, B. 1975, *Icarus*, **25**, 104
 Clark, B. E., Bus, S. J., Rivkin, A. S., Shepard, M. K., & Shah, S. 2004, *AJ*, **128**, 3070
 DeMeo, F. E., Binzel, R. P., Slivan, S. M., & Bus, S. J. 2009, *Icarus*, **202**, 160
 Devogèle, M., Tanga, P., Cellino, A., et al. 2018, *Icarus*, **304**, 31
 Dollfus, A., Mandeville, J. C., & Duseaux, M. 1979, *Icarus*, **37**, 124
 Dollfus, A., Wolff, M., Geake, J. E., Lupishko, D. F., & Dougherty, L. M. 1989, in *Asteroids II*, eds. R. P. Binzel, T. Gehrels, & M. S. Matthews, 594
 Elkins-Tanton, L. T., Asphaug, E., Bell, J. F., et al. 2020, *J. Geophys. Res. (Planets)*, **125**, e06296
 Fornasier, S., Clark, B. E., Dotto, E., et al. 2010, *Icarus*, **210**, 655
 Fornasier, S., Clark, B. E., & Dotto, E. 2011, *Icarus*, **214**, 131

- Gil-Hutton, R. 2007, *A&A*, **464**, 1127
- Gil-Hutton, R. 2017, *Catalogue of asteroid polarization curves*, presented at Asteroid, Comets, Meteors 2017, Montevideo, Uruguay
- Gil-Hutton, R., & García-Migani, E. 2017, *A&A*, **607**, A103
- Gil-Hutton, R., López-Sisterna, C., & Calandra, M. F. 2017, *A&A*, **599**, A114
- Hardersen, P. S., Gaffey, M. J., & Abell, P. A. 2005, *Icarus*, **175**, 141
- Hardersen, P. S., Cloutis, E. A., Reddy, V., Mothé-Diniz, T., & Emery, J. P. 2011, *Meteorite Planet Sci*, **46**, 1910
- Jockers, K., Credner, T., Bonev, T., et al. 2000, *Kinematika i Fiz. Nebesnykh Tel Suppl.*, **3**, 13
- Kaasalainen, S., Piironen, J., Kaasalainen, M., et al. 2003, *Icarus*, **161**, 34
- Lazzaro, D., Angeli, C. A., Carvano, J. M., et al. 2004, *Icarus*, **172**, 179
- Lupishko, D. F. 2018, *Solar Syst. Res.*, **52**, 98
- Lupishko, D. 2019, *NASA Planet. Data Syst.*, 1
- Lupishko, D. F., & Belskaya, I. N. 1989, *Icarus*, **78**, 395
- Magalhaes, A. M., Rodrigues, C. V., Margoniner, V. E., Pereyra, A., & Heathcote, S. 1996, in *Astronomical Society of the Pacific Conference Series, Polarimetry of the Interstellar Medium*, eds. W. G. Roberge, & D. C. B. Whittet, 97, 118
- Mainzer, A. K., Bauer, J. M., Cutri, R. M., et al. 2016, *NASA Planetary Data System*, EAR
- Masiero, J. R., Mainzer, A. K., Grav, T., et al. 2011, *ApJ*, **741**, 68
- Muironen, K., Penttilä, A., Cellino, A., et al. 2009, *Meteorit Planet Sci*, **44**, 1937
- Neeley, J. R., Clark, B. E., Ockert-Bell, M. E., et al. 2014, *Icarus*, **238**, 37
- Ockert-Bell, M. E., Clark, B. E., Shepard, M. K., et al. 2008, *Icarus*, **195**, 206
- Ockert-Bell, M. E., Clark, B. E., Shepard, M. K., et al. 2010, *Icarus*, **210**, 674
- Ostro, S. J., Campbell, D. B., & Shapiro, I. I. 1985, *Science*, **229**, 442
- Piirola, V., Berdyugin, A., & Berdyugina, S. 2014, *SPIE Confer. Ser.*, **9147**, 914781
- Piirola, V., Berdyugin, A., Frisch, P. C., et al. 2020, *A&A*, **635**, A46
- Rivkin, A. S., Howell, E. S., Britt, D. T., et al. 1995, *Icarus*, **117**, 90
- Rivkin, A. S., Howell, E. S., Lebofsky, L. A., Clark, B. E., & Britt, D. T. 2000, *Icarus*, **145**, 351
- Shepard, M. K., Clark, B. E., Nolan, M. C., et al. 2008, *Icarus*, **195**, 184
- Shepard, M. K., Clark, B. E., Ockert-Bell, M., et al. 2010, *Icarus*, **208**, 221
- Shepard, M. K., Taylor, P. A., Nolan, M. C., et al. 2015, *Icarus*, **245**, 38
- Tholen, D. J. 1989, in *Asteroids II*, eds. R. P. Binzel, T. Gehrels, & M. S. Matthews, 1139
- Usui, F., Kuroda, D., Müller, T. G., et al. 2011, *PASJ*, **63**, 1117
- Vernazza, P., Brunetto, R., Binzel, R. P., et al. 2009, *Icarus*, **202**, 477
- Vernazza, P., Ferrais, M., Jorda, L., et al. 2021, *A&A*, **654**, A56
- Zellner, B., & Gradie, J. 1976, *AJ*, **81**, 262
- Zellner, B., Leake, M., Lebertre, T., Duseaux, M., & Dollfus, A. 1977, *Lunar Planet. Sci. Conf. Proc.*, **1**, 1091